Antifungal Agents. 10. New Derivatives of 1-[(Aryl)[4-aryl-1*H*-pyrrol-3-yl]methyl]-1*H*-imidazole, Synthesis, Anti-*Candida* Activity, and Quantitative Structure−Analysis Relationship Studies

Andrea Tafi,[†] Roberta Costi,[‡] Maurizio Botta,[†] Roberto Di Santo,[‡] Federico Corelli,[†] Silvio Massa,[†] Andrea Ciacci,[†] Fabrizio Manetti,[†] and Marino Artico*[,‡]

Dipartimento Farmaco Chimico Tecnologico, Università di Siena, Via Aldo Moro, S. Miniato, I-53100 Siena, Italy, "Istituto Pasteur-Fondazione Cenci Bolognetti", Dipartimento di Studi Farmaceutici, Facoltà di Farmacia, Università di Roma "La Sapienza", P.le Aldo Moro 5, I-00185 Roma, Italy

Received November 2, 2001

The synthesis, anti-*Candida* activity, and quantitative structure−activity relationship (QSAR) studies of a series of 2,4-dichlorobenzylimidazole derivatives having a phenylpyrrole moiety (related to the antibiotic pyrrolnitrin) in the α-position are reported. A number of substituents on the phenyl ring, ranging from hydrophobic (*tert*-butyl, phenyl, or 1-pyrrolyl moiety) to basic (NH_2), polar (CF_3, CN, SCH_3, NO_2), or hydrogen bond donors and acceptor (OH) groups, were chosen to better understand the interaction of these compounds with cytochrome P450 14-α-lanosterol demethylase ($P450_{14DM}$). Finally, the triazole counterpart of one of the imidazole compounds was synthesized and tested to investigate influence of the heterocyclic ring on biological activity. The in vitro antifungal activities of the newly synthesized azoles **10p**−**v**,**x**−**c′** were tested against *Candida albicans* and *Candida* spp. at pH 7.2 and pH 5.6. A CoMFA model, previously derived for a series of antifungal agents belonging to chemically diverse families related to bifonazole, was applied to the new products. Because the results produced by this approach were not encouraging, Catalyst software was chosen to perform a new 3D-QSAR study. Catalyst was preferred this time because of the possibility of considering each compound as a collection of energetically reasonable conformations and of considering alternative stereoisomers. The pharmacophore model developed by Catalyst, named HYPO1, showed good performances in predicting the biological activity data, although it did not exhibit an unequivocal preference for one enantiomeric series of inhibitors relative to the other. One aromatic nitrogen with a lone pair in the ring plane (mapped by all of the considered compounds) and three aromatic ring features were recognized to have pharmacophoric relevance, whereas neither hydrogen bond acceptor nor hydrophobic features were found. These findings confirmed that the key interaction of azole antifungals with the demethylase enzyme is the coordination bond to the iron ion of the porphyrin system, while interactions with amino acids localized in proximity of heme could modulate the biological activity of diverse antifungal agents. In conclusion, HYPO1 conveys important information in an intuitive manner and can provide predictive capability for evaluating new compounds.

Introduction

Azole antifungal agents are useful drugs and are widely used for the treatment of topic or inner mycoses, in particular AIDS-related mycotic pathologies.[1−4] It is well-known that azole derivatives block ergosterol biosynthesis, causing its depletion and accumulation of lanosterol and some other 14-methylsterols[5−7] (Chart 1). Such sterols alter membrane fluidity with concomitant reduction in the activity of membrane-associated enzymes, increased permeability, and inhibition of cell growth and replication.[8−9]

The first step of ergosterol biosynthesis is the demethylation of lanosterol performed by 14-α-lanosterol demethylase ($P450_{14DM}$, CYP51), a member of the enzyme cytochrome P450 dependent superfamily,[10,11] which catalyzes the removal of 14-α-methyl group of lanosterol. Crossover inhibition of CYP51 in different species is assumed to cause undesirable side effects and is one of the reasons for the search of better, more selective agents.

Chart 1. Natural Sterols

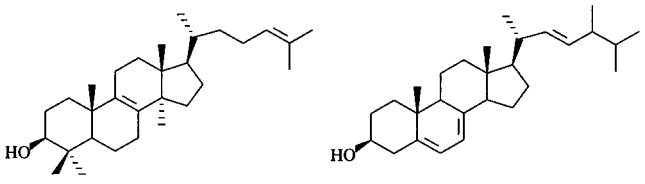

Lanosterol Ergosterol

The problem of specificity is commonly addressed empirically by applying computer simulation techniques such as receptor fitting and receptor mapping. In the first approach, the development of structural models for the active site of enzymes (based on primary sequence analyses and modeling by homology) is exploited. The structures of a number of P450-dependent enzymes

* To whom correspondence should be addressed. Phone and fax: +39-6-4462731. E-mail: marino.artico@uniroma1.it.
[†] Università di Siena.
[‡] Università di Roma "La Sapienza.

10.1021/jm011087h CCC: $22.00
Published on Web 05/29/2002

Chart 2. Azole Antifungal Agents Used in Clinical Practice

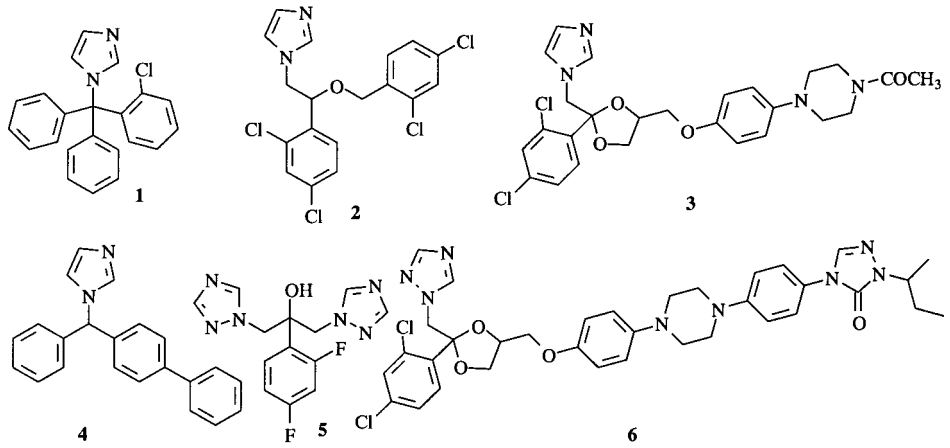

belonging to prokaryotic microorganisms, such as P450cam from *Pseudomonas putida*,[12] P450eryF from *Saccaropolyspora erythrea*,[13] and P450ter from *Pseudomonas* sp.,[14] have been elucidated, while only the crystal structure of a CYP51 cytochrome, a soluble orthologue from *Mycobacterium tuberculosis* (MTCYP51), is available until now.[15] Despite a limited sequence identity (generally 10−30%), all cytochromes P450 show very similar secondary and tertiary structures; consequently, homology modeling studies have been performed in the past few years, starting from 3D structures of the above-mentioned prokaryotic enzymes.[16−18]

A pure, indirect approach focusing mainly on structural and physicochemical properties of active and inactive compounds (receptor mapping) has been applied in recent years[19,20] to identify structure−activity relationships helpful for designing new, more specific drug candidates and eventually for understanding the enzyme active-site topography. Both of the above-mentioned theoretical approaches have reached similar conclusions concerning structure−activity relationships, indicating that the binding of azole antifungal agents involves a principal interaction between the azole ring and the CYP51 heme moiety. There are additional and mainly lypophilic ($\pi-\pi$ stacking and steric) interactions within the heme environment. Supplementary interactions with residues of the substrate channel access have also been invoked, even though they are not relevant for activity, in the case of inhibitors such as ketoconazole.[16] In the case of fluconazole interacting with MTCYP51, this overall scenario has only just been confirmed; the inhibitor, in fact, has been found to coordinate with the iron ion and to show a few further nonbonded contacts with residues of the active-site chamber.[15]

Since the identification of clotrimazole (**1**)[21] in 1972, a number of antifungal azole agents were studied and are now used in clinical practice. Miconazole (**2**) and related derivatives, together with ketoconazole (**3**)[22,23] and bifonazole (**4**),[24] belong to the class of imidazoles; fluconazole (**5**) and itraconazole (**6**) are the most important drugs of the triazole family[1−4] (Chart 2).

Our decennial interest in antifungal drugs,[19,25−36] led us to the discovery of potent antimycotic compounds belonging to azolyl diaryl ethane **7**[26,32,35] or azolyl diaryl methane groups **8**, **9**, and **10a**−**o**.[19,27−30,33,34] In the latter class, 1-[(aryl)[4-aryl-1*H*-pyrrol-3-yl]methyl]-1*H*-imidazoles[27,34] showed the highest activity in either in vitro or in vivo tests and compounds **10a** and **10o** were found to be effective against experimental cutaneous candidosis (*C. albicans* A170 strain) produced in albino female rabbits with topical efficacy higher or comparable to that of bifonazole, used as a reference drug.[34] In this research, we synthesized and tested a number of derivatives substituted on the aryl moiety of the benzylimidazole group with a halogen, methyl, amino, or nitro group. In particular, the 2,4-dichloro compound proved to lead to the most active compounds.[34]

Now we describe the synthesis, anti-*Candida* activity, and 3D quantitative structure−activity relationship (QSAR) studies of a series of 2,4-dichlorobenzylimidazole derivatives **10p**−**c′** linked in the α-position to a phenylpyrrole moiety related to the antibiotic pyrrolnitrin. A number of groups, ranging from hydrophobic (*tert*-butyl, phenyl, or 1-pyrrolyl moiety) to basic (NH_2), polar (CF_3, CN, SCH_3, NO_2), or hydrogen-bonding groups (OH), were chosen as substituents on the phenyl ring to get an insight on the influence of the substitution pattern on biological activity. Finally, the triazole counterpart of **10o** (namely, compounds **10b′** and **10c′**) was synthesized and tested (Chart 3). A pharmacophore model was developed in order to explain the structure−activity relationships of the new derivatives **10p**−**c′** and of the antifungals **4** and **7a**−**10o**. Catalyst software was preferred to perform the 3D-QSAR study mainly because of the opportunity it gave to consider each compound as a collection of energetically reasonable conformations and to consider alternative stereoisomers.

Chemistry

Compounds **10p**−**c′** were synthesized as depicted in Schemes 1−3. Azolyl derivatives **10p**−**s**,**y**−**c′** were obtained by the annulation of toluene-4-sulfonylmethylisocyanide (TosMIC) with the properly substituted chalcones **11a**−**d**,**g**,**h**, in the presence of sodium hydride as a catalyst, to give 4-aryl-3-aroyl pyrroles **12a**−**d**,**i**,**j**. Compounds **11a**−**d**,**g**,**h**, employed as starting material, were synthesized by condensation of the 2,4-dichloroacetophenone with substituted benzaldehydes in the presence of aqueous sodium hydroxide.

Alkylation of the known pyrrole **12j**[34] with methyl or ethyl iodide in alkaline medium (K_2CO_3) gave *N*-alkylpyrrolyl methanones **12k** or **12l**, respectively, and

Chart 3. Newly Synthesized Derivatives **10p**−**c** and Azoles **7**−**9** and **10a**−**o** Used in the QSAR Studies

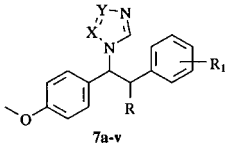

7a-v

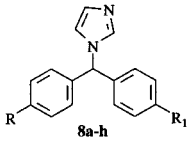

8a-h

7a	R=H	R_1=4-Cl	X = CH	Y = CH
7b	R=H	R_1=2,4-Cl_2	X = CH	Y = CH
7c	R=H	R_1=4-NH_2	X = CH	Y = CH
7d	R=H	R_1=3-(1-pyrrolyl)	X = CH	Y = CH
7e	R=H	R_1=4-Cl	X = CH	Y = N
7f	R=H	R_1=2-Cl	X = CH	Y = CH
7g	R=H	R_1=3-F	X = CH	Y = CH
7h	R=H	R_1=2-NO_2	X = CH	Y = CH
7i	R=H	R_1=4-OMe	X = CH	Y = N
7j	R=H	R_1=2-(1-pyrrolyl)	X = CH	Y = CH
7k	R=H	R_1=4-NO_2	X = CH	Y = CH
7l	R=H	R_1=4-OMe	X = CH	Y = CH
7m	R=H	R_1=2-Cl	X = N	Y = CH
7n	R=Et	R_1=4-NO_2	X = CH	Y = CH
7o	R=2,4-Cl_2-Bn	R_1=4-OMe	X = CH	Y = CH
7p	R=2,4-Cl_2-Bn	R_1=4-Cl	X = N	Y = CH
7q	R=H	R_1=3-Cl	X = CH	Y = CH
7r	R=H	R_1=2-F	X = CH	Y = CH
7s	R=H	R_1=4-F	X = CH	Y = CH
7t	R=Et	R_1=4-Cl	X = N	Y = CH
7u	R=Et	R_1=4-Cl	X = CH	Y = N
7v	R=2,4-Cl_2-Bn	R_1=4-Cl	X = CH	Y = CH

8a	R=H	R_1=1-pyrrolyl
8b	R=H	R_1=NO_2
8c	R=Me	R_1=1-pyrrolyl
8d	R=Me	R_1=2,4-Cl_2-BzNH
8e	R=Cl	R_1=NO_2
8f	R=Me	R_1=NO_2
8g	R=Cl	R_1=1-pyrrolyl
8h	R=H	R_1=NH_2

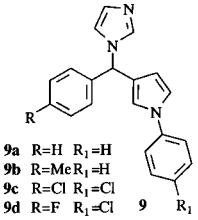

9

9a	R=H	R_1=H
9b	R=Me	R_1=H
9c	R=Cl	R_1=Cl
9d	R=F	R_1=Cl
9e	R=H	R_1=Cl
9f	R=Me	R_1=F
9g	R=Cl	R_1=F
9h	R=H	R_1=F
9i	R=F	R_1=H
9j	R=Me	R_1=Cl
9k	R=F	R_1=F

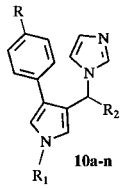

10a-n

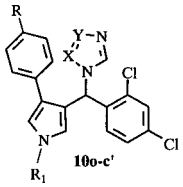

10o-c'

10a	R=Cl	R_1=H	R_2=Ph	
10b	R=Cl	R_1=Me	R_2=Ph	
10c	R=F	R_1=H	R_2=Ph	
10d	R=OMe	R_1=2,4-Cl_2-Bn	R_2=Ph	
10e	R=H	R_1=2,4-Cl_2-Bn	R_2=Ph	
10f	R=Cl	R_1=2,4-Cl_2-Bn	R_2=Ph	
10g	R=H	R_1=H	R_2=1-naphthyl	
10h	R=H	R_1=H	R_2=2-naphthyl	
10i	R=H	R_1=Me	R_2=2-naphthyl	
10j	R=Me	R_1=Me	R_2=Ph	
10k	R=H	R_1=Me	R_2=Ph	
10l	R=Me	R_1=2,4-Cl_2-Bn	R_2=Ph	
10m	R=F	R_1=Me	R_2=Ph	
10n	R=H	R_1=Me	R_2=1-naphthyl	

10o	R=Cl	R_1=H	X=CH	Y=CH
10p	R=*tert*-Bu	R_1=H	X=CH	Y=CH
10q	R=Ph	R_1=H	X=CH	Y=CH
10r	R=CF_3	R_1=H	X=CH	Y=CH
10s	R=CN	R_1=H	X=CH	Y=CH
10t	R=NO_2	R_1=H	X=CH	Y=CH
10u	R=NH_2	R_1=H	X=CH	Y=CH
10v	R=1-pyrrolyl	R_1=H	X=CH	Y=CH
10w	R=OTHP	R_1=H	X=CH	Y=CH
10x	R=OH	R_1=H	X=CH	Y=CH
10y	R=SMe	R_1=H	X=CH	Y=CH
10z	R=Cl	R_1=Me	X=CH	Y=CH
10a'	R=Cl	R_1=Et	X=CH	Y=CH
10b'	R=Cl	R_1=H	X=N	Y=CH
10c'	R=Cl	R_1=H	X=CH	Y=N

sodium borohydride reduction of ketones **12a**−**d**,**i**−**l** in a refluxing tetrahydrofuran/water mixture afforded the corresponding carbinols **13a**−**d**,**h**−**k**. The latter compounds were treated with 1,1′-carbonyldiimidazole to give imidazoles **10p**−**s**,**y**−**a**′, while reaction of derivative **13i** with 1,1′-carbonylditriazole, led to a mixture of 1,2,4- and 1,3,4-triazolyl isomers **10b**′ and **10c**′, which were separated by column chromatography (Scheme 1).

The synthesis of hydroxy derivative **10x** is depicted in Scheme 2. The required basic reaction conditions of the two first steps forced us to a preliminary protection of the hydroxy group. For this, 4-hydroxybenzaldehyde was first treated with 2,3-dihydro-2*H*-pyran in the presence of pyridinium *p*-toluenesulfonate (PPTS) as a catalyst to afford 4-(tetrahydro-2-pyranyloxy)benzaldehyde, which was then condensed with (2,4-dichlorophenyl)ethanone in alkaline medium (barium hydroxide), leading to the chalcone **11f**. The TosMIC reaction, sodium borohydride reduction, and CDI treatment in turn led to protected imidazole derivatives **10w**, which was then treated with *p*-toluenesulfonic acid to afford imidazole **10x**.

Scheme 1[a]

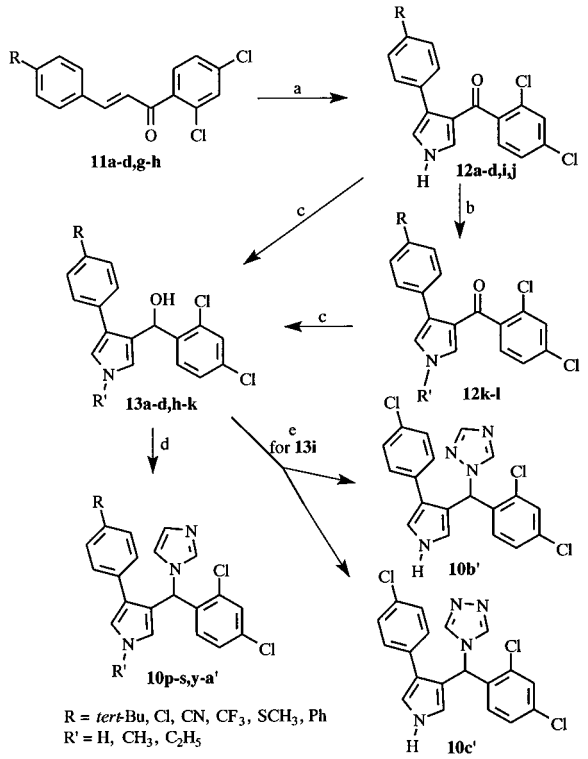

[a] Reagents: (a) tosylmethylisocyanide (TosMIC), NaH, DMSO, Et_2O; (b) alkyl iodide, K_2CO_3, DMF; (c) $NaBH_4$, THF, H_2O; (d) 1,1′-carbonyldiimidazole (CDI), MeCN; (e) 1,1′-carbonylditriazole, MeCN.

Scheme 2[a]

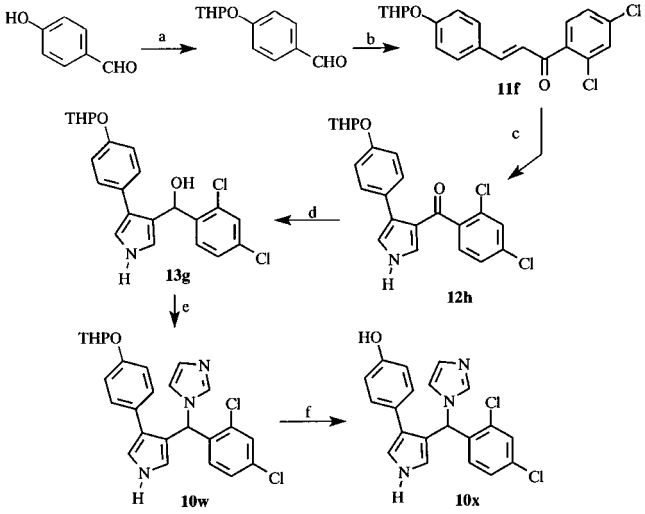

[a] Reagents: (a) dihydropyran, PPTS; (b) 1-(2,4-dichlorophenyl)-ethanone, $Ba(OH)_2$, MeOH; (c) tosylmethylisocyanide (TosMIC), NaH, DMSO, Et_2O; (d) $NaBH_4$, THF, H_2O; (e) 1,1′-carbonyldiimidazole (CDI) MeCN; (f) PTSA, MeOH.

The synthetic pathway for derivatives **10t**−**v** is reported in Scheme 3. Sodium borohydride reduction of methanone **12e**, in turn prepared by reaction of TosMIC with nitrochalcone **11e**, gave the corresponding carbinol **13e**, which was then reacted with CDI to furnish imidazole **10t**. Catalytic hydrogenation of the latter compound with hydrogen in the presence of 5% palladium on charcoal provided the amino derivative **10u**, while tin chloride reduction in acidic medium of **12e** led to amino methanone **12f**, which was treated with 2,5-

Scheme 3[a]

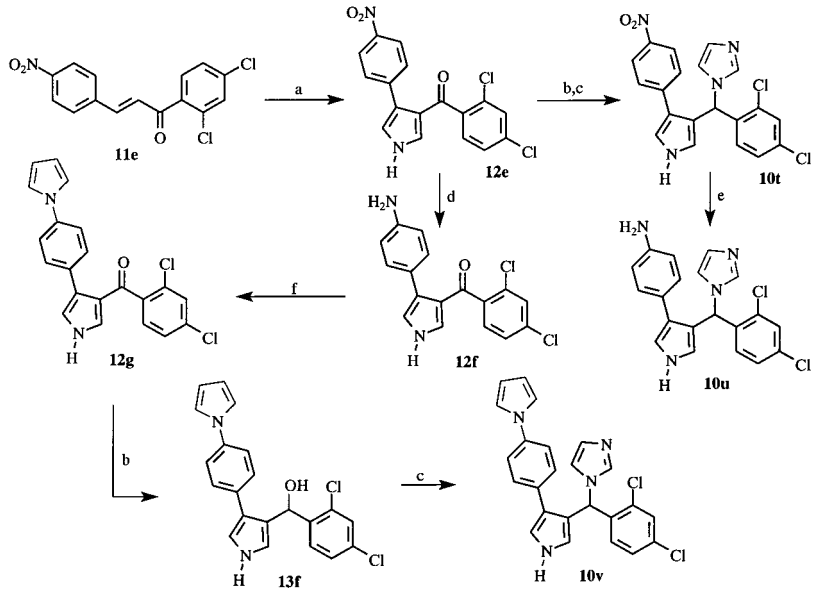

[a] Reagents: (a) tosylmethylisocyanide (TosMIC), NaH, DMSO, Et_2O; (b) $NaBH_4$, THF, H_2O; (c) 1,1′-carbonyldiimidazole (CDI), MeCN; (f) PTSA, MeOH; (d) $SnCl_2$, HCl, EtOH; (e) H_2, Pd/C, AcOEt; (f) 2,5-dimethoxytetrahydrofuran, AcOH.

Table 1. IR and ^{1}H NMR Spectra of Azole Derivatives **10p**−**c**′

compd	IR, cm^{-1}	^{1}H NMR solvent	^{1}H NMR, δ
10p	3110 (NH)	$CDCl_3$	1.30 (9H, s, CH_3), 6.28 (1H, m, pyrrole Cα-H), 6.57−7.47 (12H, m, pyrrole Cα-H, imidazole H, benzene H and CH), 8.96 (1H, bs, NH)
10q	3100 (NH)	$CDCl_3$	6.31 (1H, m, pyrrole Cα-H), 6.77−6.99 (4H, m, pyrrole Cα-H, benzene H and CH), 7.10−7.60 (14H, m, imidazole H and benzene H), 8.73 (1H, bs, NH)
10r	3110 (NH)	DMSO-d_6	6.28 (1H, m, pyrrole Cα-H), 8.79 (1H, d, J_o = 8.4 Hz, benzene H), 6.94 (3H, m, imidazole C4−H and C5−H and benzene H), 7.11 (1H, s, CH), 7.23 (1H, m, pyrrole Cα-H), 7.34−7.45 (3H, m, benzene H), 7.58−7.63 (4H, m, imidazole C2−H and benzene H), 11.33 (1H, bs, NH)
10s	3100 (NH), 2210 (CN)	DMSO-d_6	6.26 (1H, m, pyrrole Cα-H), 6.77 (1H, d, J_o = 8.4 Hz, benzene H), 6.96 (2H, m, benzene H), 7.10 (1H, s, CH), 7.28−7.44 (4H, m, imidazole C4−H and C5−H and benzene H), 7.63−7.72 (4H, m, pyrrole Cα-H, imidazole C2−H and benzene H), 11.37 (1H, bs, NH)
10t	3100 (NH)	DMSO-d_6	6.28 (1H, d, J_{o1} = 8.4 Hz, benzene H), 6.94−7.11 (3H, m, imidazole C4−H and C5−H and CH), 7.37−7.48 (4H, m, pyrrole Cα-H and benzene H), 7.65 (1H, s, imidazole C2-H), 8.10 (2H, d, J_{o2} = 8.8 Hz, benzene H near nitro group), 11.46 (1H, bs, NH)
10u	3410, 3320, 3110 (NH_2, NH)	$CDCl_3$	1.77 (2H, bs, NH_2), 6.25 (1H, m, pyrrole Cα-H), 6.59−7.44 (12H, m, pyrrole Cα-H, imidazole H, benzene H and CH), 8.44 (1H, bs, NH)
10v	3110 (NH)	DMSO-d_6	6.24 (3H, m, pyrrole Cα-H), 6.78−7.50 (13H, m, pyrrole Cα-H, imidazole C4−H and C5−H, benzene H and CH), 7.62 (1H, m, imidazole C2−H), 11.19 (1H, bs, NH)
10x	3300, 3110 (OH, NH)	$CDCl_3$	6.21 (1H, m, pyrrole Cα-H), 6.66−6.83 (7H, m, imidazole C4−H and C5−H, benzene H and CH), 6.92 (1H, m, pyrrole Cα-H), 7.11−7.38 (3H, m, benzene H), 7.53 (1H, m, imidazole C2−H), 8.50 (1H, bs, NH)
10y	3100 (NH)	DMSO-d_6	3.38 (3H, s, CH_3), 6.25 (1H, m, pyrrole Cα-H), 6.77−7.63 (12H, m, pyrrole Cα-H, imidazole H, benzene H and CH), 11.12 (1H, bs, NH)
10z		$CDCl_3$	3.66 (3H, s, CH_3), 6.11 (1H, d, $J_{2,5}$ = 2.2 Hz, pyrrole Cα-H), 6.69−7.42 (11H, m, pyrrole Cα-H, imidazole C4−H and C5−H, benzene H and CH), 7.48 (1H, m, imidazole C2−H)
10a′		$CDCl_3$	1.42 (3H, t, CH_3), 3.87 (2H, q, CH_2), 6.12 (1H, m, pyrrole Cα-H), 6.66−7.44 (12H, m, pyrrole Cα-H, imidazole H, benzene H and CH)
10b′	3110 (NH)	$CDCl_3$	6.11−7.40 (12H, m, pyrrole Cα-H, imidazole C3−H, benzene H and CH), 7.93 (1H, m, imidazole C5−H), 8.23 (1H, bs, NH)
10c′	3110 (NH)	$CDCl_3$	6.40 (1H, m, pyrrole Cα-H), 6.77−7.41 (9H, pyrrole Cα-H and benzene H), 7.97 (1H, d, $J_{2,5}$ = 4.0 Hz, imidazole C2−H and C5−H), 8.89 (1H, bs, NH)

dimethoxytetrahydrofuran in boiling acetic acid, according to the Clauson−Kaas procedure, to give pyrrole derivative **12g**. Finally, sodium borohydride reduction of **12g** afforded the corresponding carbinol **13f**, which on treatment with CDI led to imidazole **10v**. The IR and NMR data of azoles **10p**−**c**′ and the chemical and physical properties of compounds **10p**−**c**′−**13** are reported in Tables 1 and 2, respectively.

Results and Discussion

Microbiology. In Vitro Anti-*Candida* Activities. The in vitro antifungal activities of the newly synthe-

Table 2. Chemical and Physical Data of Derivatives **10p**−**c′** and **11**−**13**[a]

compd	R	R′	X	Y	mp (°C)	recryst[b] solvent	yield (%)	reaction time (h)	chromatogr.[c] system
10p	*tert*-Bu	H	CH	CH	198−200	a	20	18	A
10q	Ph	H	CH	CH	233−235	b	43	1.5	A
10r	CF_3	H	CH	CH	235−236	c	100	18	
10s	CN	H	CH	CH	208−210	b	95	2.5	
10t	NO_2	H	CH	CH	219−221	d	77	1.5	A
10u	NH_2	H	CH	CH	183−185	d	81	15	
10v	pyrrol-1-yl	H	CH	CH	232−234	b	80	1	
10w	OTHP	H	CH	CH	204−205	c	37	0.5	
10x[d]	OH	H	CH	CH	120−122	c	71	2	A
10y	SCH_3	H	CH	CH	227−229	b	68	0.5	A
10z	Cl	CH_3	CH	CH	155−157	a	44	0.5	A
10a′	Cl	C_2H_5	CH	CH	142−144	a	62	1	A
10b′[e]	Cl	H	N	CH	130−132	c	24	3.5	B
10c′[f]	Cl	H	CH	N	106−108	c	54	3.5	B
11a	*tert*-Bu				oil		100	1.5	
11b	Ph				117−119	b	62	1	
11c	CF_3				44−46	e	100	0.5	
11d	CN				165−167	b	100	0.5	
11e[g]	NO_2				150−152	b	43	0.5	
11f	OTHP				oil		52	1	C
11g	SCH_3				115−117	b	74	1	
11h[a]	Cl								
12a	*tert*-Bu	H			220−222	a	27	0.5	D
12b	Ph	H			262−264	f	84	1	
12c	CF_3	H			228−230	b	77	0.5	
12d	CN	H			194−196	b	44	0.5	
12e	NO_2	H			203−205	b	59	0.5	D
12f	NH_2	H			255−257	b	45	120	D
12g	pyrrol-1-yl	H			242−243	b	70	0.5	A
12h	OTHP	H			240−242	f	44	1	
12i	SCH_3	H			231−233	f	74	0.5	
12j[a]	Cl	H							
12k	Cl	CH_3			oil		97	18	
12l	Cl	C_2H_5			155−157	a	48	16	D
13a	*tert*-Bu	H			65−67	e	53	30	
13b	Ph	H			130 dec	a	97	6.5	
13c	CF_3	H			66−68	e	100	8	
13d	CN	H			177−179	b	100	16	
13e	NO_2	H			162−164	c	100	17	
13f	pyrrol-1-yl	H			168−170	c	100	17	
13g	OTHP	H			103−105	a	100	24	
13h	SCH_3	H			149−150	g	94	12	
13i[a]	Cl	H							
13j	Cl	CH_3			oil		94	1.5	
13k	Cl	C_2H_5			124−126	e	93	0.5	

[a] Data of known derivatives **11h**, **12j**, **13i** are reported in ref 34. [b] Recrystallization solvents: (a) benzene/cyclohexane; (b) ethanol; (c) benzene; (d) *iso*-propanol; (e) cyclohexane; (f) *N*,*N*′-dimethylformamide/water; (g) toluene. [c] Chromatographic system silica gel: (A) aluminum oxide/ethyl acetate; (B) silica gel/ethyl acetate: (C) silica gel, *n*-hexane/ethyl ether 1:1; (D) aluminum oxide/chloroform. [d] Nitrate salt, mp 87−89 °C (ethanol/ethyl ether). [e] Nitrate salt, mp 224−226 °C (*iso*-propanol/*iso*-propyl ether). [f] Nitrate salt, mp 226−227 °C (ethanol/ethyl ether). [g] Reference 44.

sized azoles **10p**−**v**,**x**−**c′** against 40 strains of *Candida albicans* and against 3 strains of *Candida* spp. (two *Candida glabrata*, one *Candida krusei*) at pH 7.2 and 5.8 are reported in Tables 3 and 4, respectively. Data refer to MIC mean values, MIC_{50}, MIC_{90}, % R (percentage of resistant species at 256 μg/mL), and the MIC range. With few exceptions, MIC_{50} and MIC values parallel the related MIC_{90} data, which were chosen for a preliminary comparison between the new derivatives and reference drugs (miconazole, ketoconazole, bifonazole, and **10o**[34]) and for QSAR studies. Antifungal experiments were carried out at pH values reproducing in the growth medium the systemic physiological conditions (pH 7.2) and the mildly acidic conditions of the skin in topical application (pH 5.8).

The majority of the newly synthesized azole derivatives inhibited the growth of all strains of *C. albicans* used for antifungal assays. % R > 0 was observed for compounds **10p**, **10u**, **10x**, **10b′**, and **10c′**.

The most potent derivative at both pH 5.8 and 7.2 was imidazole **10a′**, which showed $MIC_{90} = 2$ μg/mL (pH = 5.8) comparable to the values of miconazole and ketoconazole and was 2-fold more potent than bifonazole ($MIC_{90} = 4$ μg/mL).

A number of azole derivatives (**10r**, **10v**, **10y**, **10z**, **10a′**) showed good MIC values ranging from 3.2 to 9.14 μg/mL (pH = 7.2) and proved to be as potent as miconazole, ketoconazole, and bifonazole (MIC = 1.16−9.26 μg/mL). The high potency of inhibition of the fungal growth shown by derivatives **10z** and **10a′** at either pH 5.8 or pH 7.2 supported the importance of N-substitution of the pyrrole ring. The chlorine atom on the phenyl group linked to the pyrrole moiety could be replaced with pyrrol-1-yl, CF_3, SCH_3, and CN groups without decreasing the antifungal activity. In contrast, the introduction of OH, NH_2, or *tert*-butyl substituents led to inactive derivatives **10p**, **10u,** and **10x** and replace-

Table 3. In Vitro Antifungal Activities of Imidazole Derivatives against *C. albicans* and *Candida* spp. (Two *C. glabrata* and One *C. krusei*) at pH 7.2

	fungi (no. of tested strains)									
	C. albicans (40)					*Candida* spp. (3)				
compd	% R	MIC (μg/mL)	MIC_{50} (μg/mL)	MIC_{90} (μg/mL)	range (μg/mL)	% R	MIC (μg/mL)	MIC_{50} (μg/mL)	MIC_{90} (μg/mL)	range (μg/mL)
10p	80	164.6	>256	>256	128 to >256	100		>256	>256	>256
10q	0	14.9	8	8	2−128	0	90.6	8	256	8−256
10r	0	7.63	4	8	4−64	0	17.3	16	32	4−32
10s	0	13.2	8	32	2−64	0	32.4	16	64	1−32
10t	0	14.7	8	8	2−256	0	56	32	128	8−128
10u	54	85	>256	>256	32−128	67	256	>256	>256	256 to >256
10v	0	4.4	2	4	1−32	0	14.13	4	32	2−32
10x	0	77.8	16	256	16−256	0	256	256	256	256−256
10y	0	9.14	4	8	4−64	0	66.6	64	128	8−128
10z	0	5.3	2	16	1−32	0	6.1	16	32	4−16
10a′	0	3.2	1	2	0.5−16	0	13.3	16	16	8−16
10b′	97	128	>256	>256	128 to >256	100		>256	>256	>256
10c′	77	164.6	>256	>256	128 to >256	100		>256	>256	>256
10o	0	2.14	2	4	0.5−32	0	5.01	8	8	0.5−8
miconazole	0	1.16	0.5	2	<0.25−16	0	0.83	1	1	0.5−1
bifonazole	0	2.44	2	4	0.5−32	0	4.16	4	8	0.5−8
ketoconazole	0	9.26	8	32	2−32	0	8.6	8	16	2−16

Table 4. In Vitro Antifungal Activities of Imidazole Derivatives against *C. albicans* and *Candida* spp. (Two *C. glabrata* and One *C. krusei*) at pH 5.8

	fungi (no. of tested strains)									
	C. albicans (40)					*Candida* spp. (3)				
compd	% R	MIC (μg/mL)	MIC_{50} (μg/mL)	MIC_{90} (μg/mL)	range (μg/mL)	% R	MIC (μg/mL)	MIC_{50} (μg/mL)	MIC_{90} (μg/mL)	range (μg/mL)
10p	97	256	>256	>256	256 to >256	100		>256	>256	>256
10q	0	10.05	8	8	4−64	0	53.3	16	128	16−128
10r	0	4.8	4	8	1−16	0	16	16	16	8−16
10s	0	41.3	8	32	4−64	0	58	64	256	8−256
10t	0	15.03	8	8	2−128	0	133.3	128	256	16−256
10u	80	219.4	>256	>256	128 to >256	67	256	>256	>256	256 to >256
10v	0	3.95	2	4	0.25−64	0	9.3	8	16	4−16
10x	26	150	32	128	32−256	67	128	>256	>256	128 to >256
10y	0	7	4	8	1−32	0	9.3	8	16	4−16
10z	0	2.54	0.5	2	0.5−4	0	4.5	2	64	1−64
10a′	0	2.36	1	2	0.25−32	0	5.33	4	8	4−8
10b′	68	209.4	>256	>256	128 to >256	100		>256	>256	>256
10c′	94	128	>256	>256	128 to >256	100		>256	>256	>256
10o	0	3.6	1	2	1−8	0	6.0	8	64	4−64
miconazole	0	0.57	0.5	2	<0.25−8	0	0.156	0.5	8	<0.25−0.25
bifonazole	0	5.85	2	4	1−8	0	4	4	32	2−32
ketoconazole	0	6.35	8	2	<0.25−32	0	6.53	32	128	<0.25−16

ment of imidazole with triazole abated antimicotic activity of **10o** (see derivatives **10b′** and **10c′**).

In general, the activity against *Candida albicans* was also confirmed against *Candida* spp. and the trends of microbiological profiles of the test derivatives were very similar. The most potent azole at both pH 5.8 and 7.2 was compound **10a′**, which showed the same activity of miconazole (MIC_{90} = 8 μg/mL at pH 5.8) and was 4- and 16-fold more potent than bifonazole and ketoconazole, respectively.

Molecular Modeling Studies. A CoMFA model was derived on a series of antifungal agents (**4**, **7a**−**10n**) belonging to chemically diverse families related to bifonazole (COMFA96 in the following).[19] Considering the structural similarities between the training and test sets of COMFA96 (listed in Chart 3 and Table 5) and antifungals **10o**−**v**,**x**−**c′**, the opportunity was taken to apply that model to perform the 3D-QSAR study of the new products and of **10o**, using them as an external test set that could further assess the predictive power of COMFA96. This experiment was allowed because the antimycotic activities of imidazole derivative **10o** and the newly synthesized azoles **10p**−**v**,**x**−**c′** were evaluated, as in the case of the compounds used to develop COMFA96, by means of the minimal inhibitory concentration (MIC). The results produced by this preliminary QSAR approach were not encouraging, since the activities of the newly synthesized molecules were mispredicted by COMFA96, as clearly indicated by the low value computed for the predictive r^2 (0.52). The poor predictive power of COMFA96, however, when applied to **10o**−**v**,**x**−**c′** was not completely unexpected. It was noted, in fact, that the new compounds represent a sort of extrapolation with respect to those used to derive COMFA96, since structural modifications have been introduced with respect to previous compounds **10**, which were not fairly sampled in that model (see Chart 3). Because of these unsatisfactory results, we resorted to another QSAR approach. Catalyst software[37] was preferred this time because of its peculiarities that allowed us to consider each compound as a collection of energetically reasonable conformations. Moreover, al-

Table 5. Number of Conformers, Enantiomer Used in the Fit Operation, and Experimental and Calculated Anti-*Candida* Activity [MIC_{90}(cpd)/MIC_{90}(bifonazole)] for All the Compounds Used in This Study

			MIC_{90} (cpd)/MIC_{90} (bifonazole)	
compd	conformers	enantiomer	experimental	predicted
4	37	*R*	1.0	1.1
7a	30	*S*	4.0	33
7b	98	*R*	3.6	3.5
7c	26	*S*	2.1	31
7d	45	*S*	58	29
7e	31	*S*	63	29
7f	61	*S*	63	30
7g	56	*S*	66	32
7h	91	*S*	123	29
7i	89	*S*	64	30
7j	39	*S*	7.2	31
7k	93	*S*	32	31
7l	107	*S*	8.0	29
7m	28	*S*	32	30
7n	44	1*R*,2*S*	7.3	26
7o	208	1*S*,2*S*	21	30
7p	205	1*R*,2*S*	62	12
7q	66	*S*	32	30
7r	56	*S*	63	30
7s	30	*S*	16	31
7t	56	*S*	29	30
7u	51	1*S*,2*S*	63	30
7v	60	1*R*,2*R*	10.5	15
8a	32	*S*	0.25	0.11
8b	16	*R*	2.2	1.6
8c	32	*S*	0.13	0.15
8d	59	*S*	0.70	0.81
8e	15	*S*	1.0	0.87
8f	20	*R*	0.50	0.66
8g	36	*R*	0.50	0.094
8h	20	*R*	2.5	1.1
9a	94	*R*	4.1	4.0
9b	76	*S*	1.0	1.4
9c	81	*S*	3.0	5.7
9d	99	*R*	1.8	4.9
9e	80	*R*	0.50	3.4
9f	44	*S*	1.9	1.3
9g	114	*R*	1.8	2.4
9h	131	*R*	4.0	3.0
9i	70	*R*	2.0	8.8
9j	61	*S*	0.89	1.6
9k	106	*R*	1.0	1.5
10a	49	*R*	0.46	1.1
10b	24	*R*	0.90	0.91
10c	60	*R*	1.0	1.4
10d	63	*R*	41	29
10e	186	*R*	22	9.0
10f	171	*R*	40	20
10j	37	*S*	3.8	6.0
10k	50	*R*	4.0	1.0
10l	152	*R*	42	29
10m	35	*R*	4.0	8.2
10o	88	*S*	0.80	1.6
10p	81	*S*	47	4.7
10q	167	*S*	5.6	4.0
10r	162	*S*	0.70	1.5
10s	203	*R*	6.3	11
10t	132	*S*	1.5	0.90
10u	94	*S*	52	9.6
10v	102	*S*	0.72	0.98
10x	96	*S*	26	8.1
10y	147	*R*	3.0	6.9
10z	91	*R*	3.0	3.5
10a′	162	*R*	2.9	13
10b′	89	*S*	49	30
10c′	73	*S*	49	30

ternative stereoisomers were automatically generated and considered by the software, since the chirality of the asymmetric center was not specified (in agreement with the synthetic pathways).[38]

The general paradigm considered for the QSAR study of compounds **10o**−**v**,**x**−**c′** with Catalyst is the following. The pharmacophoric model was developed taking into consideration only compounds used to derive COMFA96 and derivatives **10o**−**v**,**x**−**c′** constituted again an external test set. In fact, a general pharmacophoric model, able to explain the structure−activity relationships of azole antifungal agents and endowed with predictive power, should not be strictly dependent on the choice of the training set (as COMFA96 apparently was). On the other hand, our choice gave us the opportunity to perform a comparison between the performances of two well-established 3D-QSAR methodologies (CoMFA and Catalyst), updating at the same time the previous CoMFA model. In summary, the chosen procedure allowed the QSAR study of compounds **10o**−**v**,**x**−**c′** as well as the evaluation of the predictive character and robustness of the new approach.

To use the Catalyst methodology at its best, the training set was redesigned: 19 among 56 compounds were selected,[19] including the most active compound **8c**, whose biological activity values spanned 3 orders of magnitude (see Experimental Section).

To build the pharmacophore hypotheses, the following chemical features were considered: aromatic nitrogen with a lone pair in the ring plane (AWLP), hydrogen bond acceptor (HBAlip), hydrophobic aliphatic (HydAl), hydrophobic aromatic (HydAr), and ring aromatic (RA).[39] Because of the molecules' rigidity and structural complexity, the hypothesis generator was constrained to report hypotheses with at least three features and to include AWLP in each pharmacophore to satisfy the key interaction between azole inhibitors and the enzyme. Azole compounds, in fact, inhibit the binding of the natural substrate lanosterol to CYP51 by coordination of the ring nitrogen atom (N-3 of imidazole and N-4 of triazole) to the sixth coordination position of the iron ion of the enzyme protoporphyrin system, as also demonstrated by a recent literature report.[15]

The 18.7 cost range over the 10 best hypotheses generated by Catalyst indicated the existence of a homogeneous set of hypotheses due to a strong signal generated by the chosen training set. Composition (in terms of chemical features necessary for activity), ranking score, and statistical parameters associated with these pharmacophore hypotheses are reported in Table 6. Because the highest scoring hypothesis is usually the most likely to yield relevant information about the pharmacophore elements of a set of compounds and because of the fact that all the better hypotheses had identical composition, hypothesis 1, characterized by the best statistical parameters, was chosen to represent the "pharmacophore model" and was selected for further evaluation (HYPO1 in the following).

In Figure 1, HYPO1 is shown, with the *S* enantiomer of **8c** (the most active compound) superimposed, as a four-feature hypothesis characterized by one aromatic nitrogen with a lone pair (AWLP) and three aromatic rings (RA1, RA2, and RA3), two of which are close to each other and are coplanar (RA2 and RA3). Activity of **8c** was correctly estimated by HYPO1 because of the fact that a complete mapping of this molecule onto the pharmacophore was possible. In detail, because of the coplanarity of the phenyl and pyrrole rings of the bulky

Table 6. Composition (Features), Cost (Bits), and Statistical Parameters (rms and Correlation) Associated with the 10 Best Hypotheses (Pharmacophore Models)

hypothesis	feature 1[a]	feature 2[a]	feature 3[a]	feature 4[a]	cost[b]	rms	correlation
1	AWLP	RA1	RA2	RA3	74.12	1.08	0.944
2	AWLP	RA1	RA2	RA3	74.18	1.09	0.943
3	AWLP	RA1	RA2	RA3	75.49	1.18	0.932
4	AWLP	RA1	RA2	RA3	75.85	1.17	0.934
5	AWLP	RA1	RA2	RA3	77.01	1.23	0.927
6	AWLP	RA1	RA2	RA3	77.76	1.18	0.936
7	AWLP	RA1	RA2	RA3	84.20	1.50	0.887
8	AWLP	RA1	RA2	RA3	85.11	1.54	0.880
9	AWLP	RA1	RA2	RA3	90.72	1.73	0.845
10	AWLP	RA1	RA2	RA3	92.86	1.80	0.832

[a] AWLP: aromatic nitrogen with lone pair feature. RA: ring aromatic feature. [b] Expressed in bits.

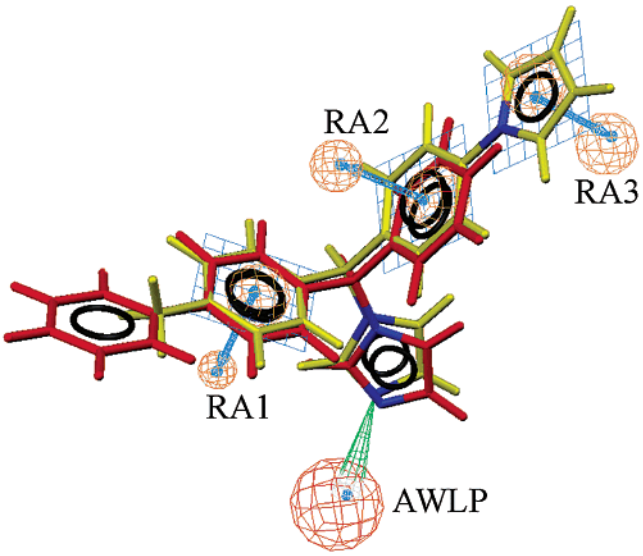

Figure 1. Compounds (*S*)-**8c** (in yellow), the most active of the whole set, and (*R*)-**4** (in red), the reference compound, mapped to the pharmacophore hypothesis HYPO1. Pharmacophore features are color-coded: red for an aromatic nitrogen with lone pair (AWLP) and orange for aromatic ring (RA1, RA2, and RA3).

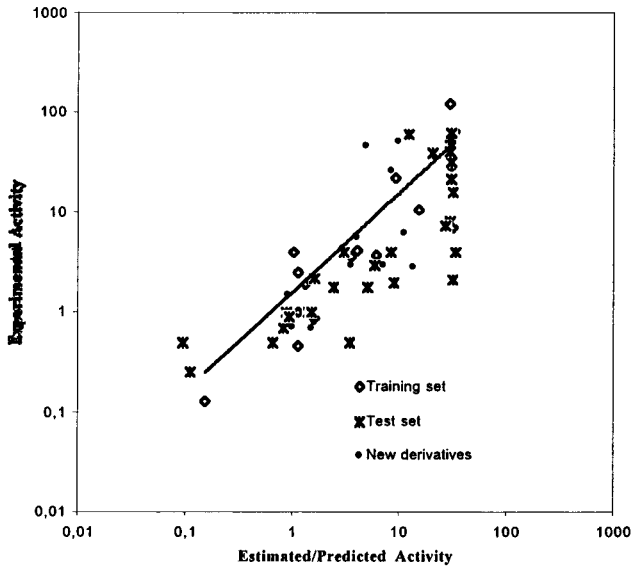

Figure 2. Regression line for HYPO1 (the pharmacophore model). Experimental versus estimated (or predicted) anti-*Candida* activity is reported for each member of the training set, of the test set, and for the new derivatives **10o**−**c′**.

4-(pyrrol-1-yl)phenyl moiety, both RA2 and RA3 were mapped. Furthermore, RA1 was mapped by **8c**'s 4-methylphenyl ring and, finally, the N-3 nitrogen atom of the imidazole ring corresponded to the AWLP feature of HYPO1. The strong inhibitory activity of **8c**, [MIC_{90}(**8c**)/MIC_{90}(**4**) = 0.13] suggests that it possesses many or all of the molecular features important for antifungal activity. Taking into account that the pharmacophore model correctly estimated the inhibitory properties of this compound (MIC_{90} = 0.15 relative to bifonazole), one may conclude that HYPO1 possibly accounts for relevant interactions between inhibitors and enzyme.

All the calculated activities from HYPO1, and the number of generated conformers for each studied molecule, are listed in Table 5, while the regression line of experimental versus estimated anti-*Candida* activities for the training set, exhibiting a correlation coefficient $r = 0.94$ and a root-mean-square deviation rms = 1.08, is shown in Figure 2. Comparison between the estimated activities of the compounds in the training set and their experimental values was, in the worst case, inferior to a 5-fold difference and, in most cases, inferior to a 2-fold difference, indicating the reliability of the model. Moreover, the cost difference between HYPO1 and the null hypothesis was 80 bits, corresponding to an about 90% chance of true correlation in the data.

Although one chiral center is present in all the molecules of the training set, HYPO1 did not exhibit a univocal preference for one enantiomeric series of inhibitors relative to the other. On the contrary, as reported in Table 5, each time a compound was superimposed on HYPO1, either the *R* or *S* enantiomer gave the best mapping according to an apparently random pattern. In the case of the reference antifungal drug **4** (bifonazole), whose best fitting onto HYPO1 is depicted in Figure 1, the *R* enantiomer showed the highest correlation between experimental and calculated activity values (1.1 estimated vs 1.0 experimental), with only three chemical features of the hypothesis, out of four, matched by the chemical groups of the ligand. The biphenyl group (bulky substituent) was found to correspond to RA1, the phenyl ring to RA2, and the N-3 nitrogen atom of the imidazole ring to the AWLP feature. Notably, (*S*)-**4** showed a conformation whose orientation on HYPO1 was similar to that depicted in Figure 1 for **8c**. This mapping gave a slightly worse activity correlation (1.2 estimated vs 1.0 experimental) with respect to the *R* enantiomer because of a worse superimposition of the chemical groups of the ligand with the pharmacophore. Notably, in a recent study by some of us devoted to the homochiral synthesis and

biological evaluation of bifonazole,[40] no differential activity between the two enantiomers of this compound was observed, and the present computational analysis confirms that unexpected result.

From an analysis of the fitting mode of the training set derivatives onto the best hypothesis, it resulted that all the ligands mapped the AWLP feature of the model, in accordance to their generally accepted mechanism of action. In general (except in the case of **8c**), compounds belonging to both classes **8** and **9** mapped three features missing RA3 (**4**, **8h**, and **9a**) or RA2 (**9f** and **9j**). Compounds belonging to class **7**, as well as those of class **10**, showed the following mapping on HYPO1: **7b**, **7v**, **10a**, **10c**, **10e**, **10j**, and **10k** matched AWLP, RA1, and RA2; **7g**, **7h**, **7j**, **7q**, **7t,** and **10l** matched only two features, missing two of the three RA's. Consequently, the three-dimensional structural properties required for an ideal CYP51A1 inhibitor can be summarized as follows: (i) an aromatic nitrogen with an accessible lone pair is strictly required (feature interacting with the iron atom of the enzyme protoporphyrin system); (ii) a diarylmethyl moiety on the azole N-1, which is preferred over a 1,2-diarylethyl; (iii) one of the two aryls on the methyl group could be better a phenyl ring with a para lypophilic substituent; (iiii) the second aryl group should be made up of two coplanar aromatic rings as in the case of **8c**.

After construction and before its application to the QSAR analysis of compounds **10o**−**v**,**x**−**c′**, the Catalyst pharmacophore was used to predict the anti-*Candida* activity values of the inhibitors used to derive COMFA96 not already included in the training set (see Experimental Section). These predictions, when compared with the corresponding observed values (see Table 5), generated a regression line that exhibited a correlation coefficient $r = 0.84$ and a root-mean-square deviation rms = 1.43 (see Figure 2). The activities of all compounds in the test set were predicted by the model to be within 0.88 log units of their actual inhibitory activities (excluding **7a** and **7c**, which showed residuals of 0.92 and 1.17 log units, respectively). In particular, the activity of (*S*)-**8a** (most active compound in the test set) against *Candida albicans* was predicted by the model to be 0.11, in good agreement with the experimentally determined value of 0.25 (residual 0.36 log units). This result accounted for the mapping of (*S*)-**8a** with all the features of the pharmacophore: the N-3 of the imidazole ring and the phenyl group mapped AWLP and RA1, respectively, while RA2 and RA3 were represented respectively by the phenyl ring and by the pyrrole ring of the bulky aromatic moiety. It is interesting to note that the *R* enantiomer was found to map only three features (namely, AWLP, RA1, and RA2) and consequently was predicted to be much less active (1.3 vs 0.25).

HYPO1 accounted for the trend of the biological data associated with class **8** and class **7** (derivatives homologous to the **8**'s with a methylene spacer) compounds in the test set. The markedly decreased inhibitory activity of compounds **7** was ascribed as being due to the unmatching of pharmacophoric features; **7n** and **7p** missed the mapping of RA3, while all other compounds were completely unable to match both RA2 and RA3 features. The model also accounted for the contribution

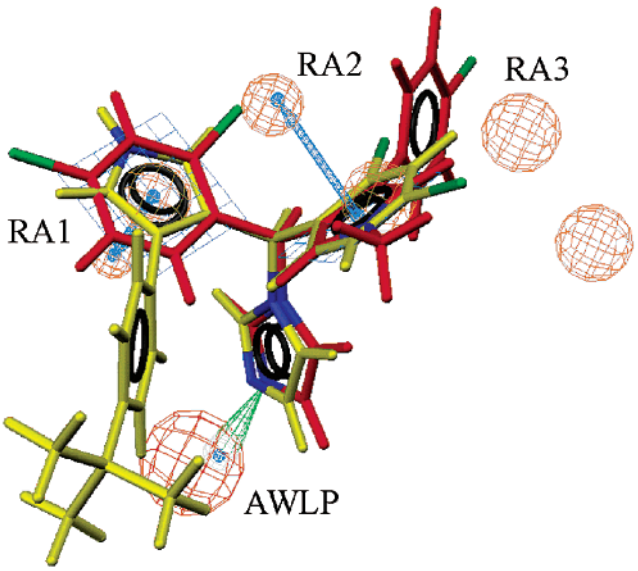

Figure 3. Compound **10p** (in yellow) and **10z** (in red) mapped to HYPO1. Pharmacophore features are color-coded: red for an aromatic nitrogen with lone pair (AWLP) and orange for aromatic ring (RA1, RA2, and RA3).

of the substituted pyrrole moiety to the inhibitory activity, as in the case of molecules in classes **9** and **10**. In particular, compounds in which the pyrrole ring has an aromatic substituent in position 4 had no conformations able to map RA3.

HYPO1 was than applied to perform the QSAR study of the compounds **10o**−**v**,**x**−**c′**. Accordingly, their anti-*Candida* activity values were predicted (see Table 5 and Figure 2) and the predicted-versus-experimental regression line was analyzed. The cited derivatives exhibited a correlation coefficient $r = 0.78$ and a root-mean-square deviation rms = 1.54 that were judged to be satisfactory. The activities of all compounds in this external test set were predicted by the model to be within 0.73 log units of their actual values (excluding **10p**, which showed a residual of 1.00 log unit). None of the new compounds fulfilled all four pharmacophoric features, and univocal preference for one enantiomeric series relative to the other was not exhibited (see Table 5) even though *S* enantiomers of the more active inhibitors were considered by the software. Compounds **10o**, **10p**, **10q**, **10r**, **10t**, **10x**, and **10v**, notwithstanding their different activity values, were superimposed by the program on HYPO1 in a similar manner. The N-3 nitrogen atom of the imidazole and the 2,4-Cl_2-phenyl substituent were placed on the AWLP and RA2 features, respectively, while the pyrrole group of the bulky aromatic substituent mapped RA1. The activities of **10o**, **10q**, **10r**, **10t**, **10x**, and **10v** were predicted to be in good agreement with the experimental values (1.6 vs 0.80, 4.0 vs 5.6, 1.5 vs 0.70, 0.90 vs 1.5, 8.1 vs 26, and 0.98 vs 0.72, respectively), while in the case of ligand **10p**, a value of 4.7 was calculated versus an actual activity of 47. The poor agreement obtained in the case of **10p**, however, could be reasonably rationalized by assigning the low experimental activity shown by this derivative to steric hindrance problems (not well understood by Catalyst[41]) of the R group (*tert*-butyl).

Inhibitors **10s**, **10u**, **10y**, **10z**, and **10a′** were characterized by an orientation into the pharmacophore model very similar to that of **8c** and by the molecular frag-

ments fulfilling all but one of the features of HYPO1 (Figure 3). In fact, the N-3 nitrogen atom of the imidazole ring mapped AWLP, and the 2,4-Cl_2-phenyl substituent mapped RA1 and the pyrrole RA2. Predicted activities of these compounds, as shown in Table 5, were in reasonable agreement with the experimentally determined values. In the case of **10u**, the derivative showed the second worst connection between experimental and calculated activities (9.6 vs 52); the deviation found might be due to the presence of a NH_2 group (R_1), which, decreasing the lypophilic characteristics of the molecule, could prevent the crossing of the membrane of the fungi cell.

As expected, and because of their low activity, triazole compounds **10b′** and **10c′** matched only two features of HYPO1, AWLP, and RA1 (with the 2,4-Cl_2-phenyl substituent), so the importance of the nature of the azole ring for the activity was demonstrated.

A further analysis of HYPO1 was devoted to understand the role played by the pyrrole ring substituents (R and R_1) on the biological activity of the compounds. The effect of these groups seemed to be related to the influence they exert on the overall 3D shape of the molecules. In the homologous series **10o**, **10z**, and **10a′**, for instance, the substitution of the hydrogen atom (**10o**) at the 1-position of the pyrrole ring with an alkyl group (R_1 = Me or Et) forced compounds **10z** and **10a′** to switch the enantiomer and the orientation mapped onto HYPO1. Particularly, in the case of **10a′**, Catalyst was unable to find a conformation (in the energetic window of 20 kcal/mol)[42] that could give a fit similar to that of **10o**. As a consequence, the match of **10a′** onto HYPO1 was slightly worse, as demonstrated by the predicted activity value of 15. The R substituent seemed to be responsible for the fine-tuning of the activity of the compounds **10q**, **10r**, **10s**, **10t**, **10v**, and **10y**, since small differences between the shape of putative bioactive conformers produce slight variations in the superposition onto HYPO1.

Conclusions

As a summary of this QSAR study, the pharmacophore model developed by Catalyst and named HYPO1 showed good performance in predicting the biological activity data of a set of inhibitors belonging to the 1-[(aryl)[4-aryl-1*H*-pyrrol-3-yl]methyl]-1*H*-imidazole class.

HYPO1 did not exhibit an unequivocal preference for one enantiomeric series of inhibitors relative to the other. On the contrary, an apparently random pattern was found. Notably, this result, even though surprising and unexpected, appears to be in agreement with recent experimental findings.[40]

The pharmacophore model postulates that there is an essential three-dimensional arrangement of functional groups that each molecule must possess to strongly inhibit the enzyme. The modulation of the activities of the compounds considered in this study resulted in a dependence mainly on the number of pharmacophoric features mapped by each one of them. Hence, our model provides both crucial information about how well the chemical features of a subject molecule overlap with the hypothesis and the ability of molecules to adjust their conformations in order to fit the enzyme with energetically reasonable conformations; only the most active compounds **8a**, **8c**, and **8g** were able to match all four features of HYPO1 because of the structural characteristics peculiar to these three compounds (possessing a completely planar phenylpyrrolyl aromatic moiety). Many compounds, showing intermediate activities, could match three features, and finally the less active inhibitors were found to match two features only, since only conformations poorly fitting the enzyme were found in the considered energy window.

One aromatic nitrogen with lone pair (mapped by all of the considered compounds) plus three aromatic ring features were recognized by HYPO1 to have pharmacophoric relevance, whereas no hydrogen bond acceptor, hydrophobic aliphatic features, and hydrophobic aromatic features were found. These findings confirmed that the key interaction of azole antifungines with the demethylase enzyme is the coordination bond with the iron ion of the porphyrine system. On the other hand, the detection of aromatic interactions only, together with the missing of hydrogen bonds, could be interpreted as due to the poor structural diversity of the studied compounds. On the contrary, because the features constituting HYPO1 were sufficient to reproduce in a satisfactory manner the activities of all the compounds in the training and test sets and to predict those of **10o**−**v**,**x**−**c′** (about 65 compounds), we believe this pharmacophore might reflect the structural characteristics of the cavity surrounding the prostethic group in the involved cytochrome. Accordingly, and as a rule, aromatic interactions with amino acids localized in proximity of heme (described by the features RA1, RA2, and RA3) could be responsible of the different activities of diverse antifungal agents, while hydrogen bonds or similar hydrophilic interactions with farther residues (not pointed out in this study) could fortuitously increase the affinity of an inhibitor with respect to another one.

Recently, a paper concerning the crystal structure of cytochrome P450 14α-sterol demethylase from *Mycobacterium tuberculosis* in complex with azole inhibitors has appeared in the literature, which indirectly supports our results. In that paper it is reported that "azole resistance in fungi develops in the protein region involved in orchestrating passage of the enzyme through the different conformational stages along the catalytic cycle rather than in residues directly contacting inhibitors" (fluconazole in that case).[15] Moreover, the active-site chamber dome in the case of fluconazole is reported to show prevalently phenylalanine residues that constitute the ceiling above the porphyrin plane (F78, M79, F83, and F255) and interact with the inhibitor. Finally, in that paper, none of the nonbonded interactions detected between the inhibitors and the enzyme is reported to play a major role in determining the binding. All these results seem to be highly compatible with HYPO1.

In conclusion, HYPO1 conveys important information in an intuitive manner and can provide predictive capability for evaluating new compounds.

Experimental Section

1. Chemistry. Melting points were determined on a Büchi 530 melting point apparatus and are uncorrected. Infrared (IR) spectra (Nujol mulls) were recorded on a Perkin-Elmer 297 spectrophotometer. ^{1}H NMR spectra of imidazole derivatives were recorded at 200 MHz on a Bruker AC 200 spectrometer

using tetramethylsilane (Me_4Si) as the internal reference standard. Column chromatographies were performed on alumina (Merck; 70−230 mesh) or silica gel (Merck; 70−230 mesh) column. All compounds were routinely checked by TLC by using aluminum-baked silica gel plates (Fluka DC-Alufolien Kieselgel 60 F_{254}) and aluminum-baked aluminum oxide plates (Fluka DC-Alufolien Kieselgel 60 F_{254}). Developed plates were visualized by UV light. Solvents were reagent grade and, when necessary, were purified and dried by standard methods. Concentration of solutions after reactions and extractions involved the use of a rotary evaporator (Büchi) operating at a reduced pressure (ca. 20 Torr). Organic solutions were dried over anhydrous sodium sulfate. Analytical results agreed to within ±0.40% of the theoretical values. All compounds were analyzed for C, H, N, and, when present, S, Cl, and F.

2. Syntheses. Specific examples presented below illustrate the general synthetic procedures.

1,3-Diaryl-2-propenones 11. These compounds were prepared according to reported procedures.[43] Chemical and physical data of newly synthesized derivatives **11a**−**d**,**f**,**g** are reported in Table 2 together with those of the known propenones **11e**[44] and **11h**.[34] **11f** was obtained as reported below starting from 4-(tetrahydropyran-2-yloxy)benzaldehyde, which was synthesized as reported elsewhere.[45]

1-(2,4-Dichlorophenyl)-3-(4-tetrahydropyran-2-yloxyphenyl)ethanone (11f). A mixture of 4-(tetrahydropyran-2-yloxy)benzaldehyde (6.9 g, 33.5 mmol) and 1-(2,4-dichlorophenyl)ethanone (6.3 g, 33.5 mmol) in methanol (180 mL) was treated with barium hydroxide octahydrate (15.8 g, 50 mmol) and heated at 50 °C for 1 h. Then the solvent was removed under reduced pressure and the residue was treated with water (200 mL) and was extracted with ethyl acetate (3 × 150 mL). The organic extracts were collected, washed with brine (2 × 150 mL), dried, and stripped of the solvent. The residue was chromatographed on a silica gel column (*n*-hexane/ethyl ether 1:1) to afford pure **11f** (6.6 g, 52% yield).

[4-(4-Biphenylyl)-1*H*-pyrrol-3-yl]-(2,4-dichlorophenyl)-methanone (12b). A solution of **11b** (5.0 g, 14.3 mmol) and toluene-4-sulfonylmethylisocyanide (2.8 g, 14.3 mmol) in a mixture of anhydrous dimethyl sulfoxide/ethyl ether (45:90 mL) was added dropwise into a well-stirred suspension of sodium hydride (60% in white oil; 2.6 g, 65 mmol) in dry ethyl ether (75 mL). After the addition, the mixture was stirred at room temperature for 40 min and then treated with water (300 mL). The formed precipitate was filtered off, and the filtrate was washed with cold ethanol and then with light petroleum ether to afford 4.7 g (84% yield) of pure **12b**.

[4-(4-Chlorophenyl)-1-ethyl-1*H*-pyrrol-3-yl]-(2,4-dichlorophenyl)methanone (12l). A well-stirred suspension of **12j** (4.5 g, 12.7 mmol), iodoethane (14.2 g, 91 mmol), and anhydrous potassium carbonate (3.5 g, 25.4 mmol) in dry *N*,*N*-dimethylformamide (20 mL) was heated at 90 °C for 16 h. After cooling, the mixture was treated with water (100 mL) and the formed precipitate was extracted with ethyl acetate (3 × 70 mL). The collected organic extracts were washed with brine (3 × 200 mL) and dried and the solvent was evaporated to afford a crude product that was chromatographed on an aluminum oxide column (chloroform as eluent) to give pure **12l** (2.3 g, 48% yield).

[4-(4-Aminophenyl)-1*H*-pyrrol-3-yl]-(2,4-dichlorophenyl)methanone (12f). The nitro derivative **12e** (3.0 g, 8.3 mmol) was added portionwise to a well-stirred solution of tin(II) chloride dihydrate (6.6 g, 29.4 mmol) in a concentrated hydrochloric acid/ethanol mixture (7:60 mL). The resulting suspension was stirred at room temperature for 120 h. After this time, the acidic solution was diluted with water (150 mL) and then was treated with 1 N NaOH until pH 8 was attained. The inorganic precipitate was filtered off, and the filtrate was concentrated under reduced pressure. The residue was extracted with ethyl acetate (3 × 100 mL), and the collected organic extracts were washed with brine (3 × 200 mL), dried, and stripped of the solvent. The residue was chromatographed on aluminum oxide to afford pure **12f** (1.2 g, 45% yield).

(2,4-Dichlorophenyl)-[4-[4-(1*H*-pyrrol-1-yl)phenyl]-1*H*-pyrrol-3-yl]methanone (12g). A solution of amine **12f** (1.0 g, 3.0 mmol) and 2,5-dimethoxytetrahydrofuran (410 mg, 3.1 mmol) in glacial acetic acid (20 mL) was refluxed for 0.5 h. After the mixture was cooled, the solvent was removed and the residue was chromatographed on aluminum oxide (ethyl acetate as eluent) to give pure **12g** (810 mg, 70% yield).

α-(2,4-Dichlorophenyl)-4-(4-trifluoromethylphenyl)-1*H*-pyrrole-3-methanol (13c). A mixture of **12c** (3.0 g, 7.8 mmol) and sodium borohydride (880 mg, 23 mmol) in a tetrahydrofuran/water mixture (200:0.7 mL/mL) was refluxed for 8 h. After cooling, the suspension was treated with water (200 mL) and concentrated under reduced pressure. The residue was extracted with ethyl acetate (3 × 100 mL), and the organic extracts were collected, washed with brine, and dried. Evaporation of the solvent gave 3.0 g (100% yield) of **13c**, which was used in the following reaction without further purification.

1-[(2,4-Dichlorophenyl)[4-(4-trifluoromethylphenyl)-1*H*-pyrrol-3-yl]methyl]-1*H*-imidazole (10r). A solution of **13c** (3.1 g, 8.0 mmol) and 1,1′-carbonyldiimidazole (5.5 g, 34 mmol) in anhydrous acetonitrile (130 mL) was stirred at room temperature for 18 h. The solvent was removed, and the residue was dissolved in ethyl acetate (150 mL). The organic solution was washed with brine (3 × 100 mL) and the solvent was evaporated to afford the pure imidazole derivative **10r** (3.9 g, 100% yield).

1-[[4-(4-Aminophenyl)-1*H*-pyrrol-3-yl](2,4-dichlorophenyl)methyl]-1*H*-imidazole (10u). The nitro derivative **10t** (600 mg, 1.5 mmol), dissolved in ethyl acetate (150 mL), was hydrogenated in the presence of 10% palladium on charcoal (240 mg) as a catalyst for 15 h in a Parr apparatus at room temperature at an initial pressure of 4 atm. The catalyst was then filtered off and the filtrate was evaporated to give 450 mg of **10u** (81% yield).

1-[(2,4-Dichlorophenyl)[4-(4-hydroxyphenyl)-1*H*-pyrrol-3-yl]methyl]-1*H*-imidazole (10x). A suspension of tetrahydropyranyl derivative **10w** (290 mg, 6.2 mmol) in methanol (50 mL) was treated with a catalytic amount of *p*-toluenesulfonic acid, and the mixture was stirred at room temperature for 2 h. After this time the solvent was removed and the residue was dissolved in ethyl acetate (50 mL). The organic phase was washed with 1 N sodium carbonate (3 × 50 mL), then was washed with brine (3 × 50 mL), and dried, and the solvent was evaporated under reduced pressure. The residue was chromatographed on aluminum oxide (ethyl acetate as eluent) to furnish pure **10x** (170 mg, 71% yield).

3. Mycology. Anti-*Candida* in Vitro Assays. Derivatives **10p**−**v**,**x**−**c′** were tested for antimycotic activities against *C. albicans* and *Candida* spp. The antifungal potency was evaluated by means of the minimal inhibitory concentration (MIC) using the serial dilution test in a liquid nutrient medium. MIC was defined as the lowest concentration of test substance at which there was no visible growth in comparison with a blank experiment after the preset incubation time. For the preparation of the dilution series, 5 mg of substance was dissolved in DMSO (1 mL) and the solution was treated on shaking with distilled water (9 mL). Further progressive double dilutions with test medium furnished the required concentrations in the range from 0.25 to 256 μg/mL. In some cases dissolution was completed by addition of a few drops of diluted hydrochloric acid. Blanks were prepared in the test medium with the above-reported quantities of water and DMSO, without adding test substance. All tested microorganisms were preliminarily incubated at 37 °C for 18 h on Sabouraud (BBL) dextrose broth and then added to media containing the antimycotic agent. Antimicrobial tests were performed on Sabouraud broth (Difco) using inocula of 10^3/mL of fungi. Readings of MICs were taken at 24 h of growth at 37 °C. MIC values were calculated by the expression $MIC = (\sum MIC_i)/s_t$, where MIC_i is the minimal inhibitory concentration values of all strains at the used concentration C_i and s_t is the total number of strains. MIC_{50} and MIC_{90} refer to MIC for 50% and 90% of strains, respectively. Strains with MIC greater than 256 μg/mL are regarded

as resistant (R) and are expressed as percentage by the equation $R(\%) = (N_t - N_s)/N_t \times 100$, where N_t is the total number of tested strains and N_s is the number of sensitive strains. Experiments were carried out at both pH 7.2 and 5.8 employing two different lots of *C. albicans* and *Candida* spp. freshly isolated from hospitalized patients (strains were identified using standard methods). The specimens used were 40 strains of *C. albicans* and 3 strains of *Candida* spp. (two *C. glabrata* and one *C. krusei*).

4. Molecular Modeling. 4.1. Pharmacophore Generation. The training set for the pharmacophore development was chosen according to the Catalyst guidelines.[41] In particular, to enhance the probability of finding a significant model, two rules were applied: (i) inclusion of the most active compound (**8c**) in the set because of the fact that Catalyst pays particular attention to this molecule when it generates the chemical features space; (ii) maximization of the kinds and relative positions (substitution pattern) of the chemical features shared by the molecules because the program recognizes the molecules as collections of chemical features and not as assemblies of atoms or bonds. Accordingly, **4**, **8c**, **8h**, **7b**, **7g**, **7h**, **7j**, **7q**, **7t**, **7v**, **9a**, **9f**, **9j**, **10a**, **10c**, **10e**, **10j**, **10k**, and **10l** were selected as the training set. Their biological activity (MIC_{90}) values span 3 orders of magnitude, with **8c** (the most active derivative) being 1024 times more active than **7h** (the less active compound). The activity data were expressed, after having converted all the μg/mL values to μmol/mL units, as [MIC_{90}(cpd)/MIC_{90}(bifonazole)] in the range between 0.13 and 123 and are reported in the fourth column of Table 5.

Compounds **10g**, **10h**, **10i**, and **10n**, bearing a naphthyl as the R group and used in COMFA96, were excluded this time by both training and test sets because their low activities had been already assigned as being due to excluded volume problems,[19] and this peculiarity is reported to be not well understood by Catalyst.[41] In other words, these molecules might have the naphthyl functionality that bumps into a portion of the enzyme, preventing close contacts of the binding functions. This assumption is strengthened by the observation that derivatives **10i** and **10n**, both possessing a methyl group that generates further steric hindrance, show the lowest activities in the subset of naphthyl compounds. From another viewpoint, because Catalyst pays particular attention to the most active compounds in the training set, excluding such inactive compounds may not generally affect the generation of the chemical feature space relevant to the experiment.

Because no experimental data on the biologically relevant conformations of the selected compounds (for example, atomic coordinates derived from X-ray crystallographic studies of their complexes with the CYP51A1) are available, we resorted to a molecular mechanics approach to build the conformational populations to be used for pharmacophore generation. By means of the Catalyst 2D−3D sketcher, a local minimum-energy conformer of each compound of the training set was built and submitted to conformational search using the "best" procedure with the aim of collecting a representative set of conformers chosen within a range of energetically reasonable conformations (CHARMm force field).[42,46] In particular, all the conformers of each compound, within a range of 20 kcal/mol with respect to the global minimum, were employed to build a set of pharmacophore hypotheses comprising all/any of the following chemical features: aromatic nitrogen with lone pair (AWLP), hydrogen bond acceptors (HBAlip), hydrophobic aliphatics (HydAl), hydrophobic aromatics (HydAr), and ring aromatics (RA). Because of the molecules' rigidity and structural complexity, the hypothesis generator was constrained to report hypotheses with at least three features and to include an aromatic nitrogen with lone pair group in each pharmacophore to satisfy the key interaction between azole inhibitors and the enzyme. Azole compounds, in fact, inhibit the binding of the natural substrate lanosterol to CYP51A1 by coordination of the ring nitrogen atom (N-3 of imidazole and N-4 of triazole) to the sixth coordination position of the iron atom of the enzyme protoporphyrin system, as also demonstrated by a recent literature report.[15]

4.2. Pharmacophore Description. As a result of the pharmacophore generation, 61.4 bits as the total fixed cost (ideal hypothesis) and 153.8 bits as the cost of the null hypothesis were found. The cost range over the 10 best generated hypotheses was 18.7 bits (Table 6), suggesting that there was a homogeneous set of hypotheses and that the signal generated by this training set was strong. Moreover, the fact that the hypotheses were much closer to the fixed cost (i.e., the cost of hypothesis 1 is 74.1) meant that the signal could be interpreted.

4.3. Pharmacophore Validation. Fischer Test. Despite the quite high range found between the costs for an ideal versus null hypotheses (92 bits) and the good difference between the costs of HYPO1 and of null hypothesis (79 bits) ensuring a 90% chance of true correlation,[41] special care was taken to test the model for chance correlation. The pharmacophore model corresponding to HYPO1 was evaluated for statistical significance using a randomization trial procedure derived from the Fischer method.[47] Experimental activities of the training set were scrambled 19 times to obtain spreadsheets with randomized activity data. A total of 19 hypothesis generation experiments were performed using the scrambled training sets, and among the 190 resulting hypotheses (10 for each computational run), none was found with lower cost than hypothesis 1. Thus, there was at least a 95% chance that hypothesis 1 represented true correlation in the data.

Acknowledgment. Thanks are due to Ministero della Sanità, Istituto Superiore di Sanità, Progetto AIDS 1999 (Grant No. 40C.8) and to Italian CNR and MURST (40%) for partial support. Microbiological tests were performed by "Istituto di Microbiologia" of Rome University "La Sapienza". Maurizio Botta thanks the Italian Research National Council (CNR target project on "Biotechnology") and the Merck Research Laboratories for the 2001 Academic Development Program (ADP) Chemistry Award. Elemental analyses were performed by Dott M. Zancato, University of Padova, Italy.

References

(1) D'Arcy, P. F.; Scott, E. M. Antifungal Agents. *Prog. Drug Res.* **1987**, *22*, 94−147.
(2) Kerridge, D. Antifungal Drugs. *Drugs Today* **1988**, *24*, 705−715.
(3) Koltin, Y. Target for Antifungal Drug Discovery. *Annu. Rep. Med. Chem.* **1990**, *25*, 141−148.
(4) Fromtling, R. A. Imidazoles as Medically Important Antifungal Agents: An Overview. *Drugs Today* **1986**, *20*, 235−349.
(5) Vanden Bossche, H.; Bellens, D.; Cools, W.; Gorrens, P. M.; Verhoeven, H.; Willemsens, G.; De Coster, R.; Beerens, D.; Haelterman, C.; Coene, M. C.; Lauwers, W.; Le Jeune, L. Cytochrome P450: Target for Itraconazole. *Drug Dev. Res.* **1986**, *8*, 287−298.
(6) Hichcock, A.; Brown, B.; Evans, E. G. V.; Adams, D. J. Cytochrome P-450-Dependent 14α-Demethylation of Lanosterol in *Candida albicans*. *Biochem. J.* **1989**, *260*, 549−556.
(7) Asai, K.; Tsuchimori, N.; Okonogi, K.; Perfect, J. R.; Gotoh, O.; Yoshida, Y. Formation of Azole-Resistant *Candida albicans* by Mutation of Sterol 14-Demethylase P450. *Antimicrob. Agents Chemother.* **1999**, *43*, 1163−1169.
(8) Adams, J. L.; Metcalf, B. W. Therapeutic Consequences of the Inhibition of Sterol Metabolism. In *Comprehensive Medicinal Chemistry*; Hansch, C., Sammes, P. G., Taylor, J. B., Eds.; Pergamon Press: Oxford, England, 1990; Vol. 2, pp 333−364.
(9) Yeagle, P. L.; Martin, R. B.; Lala, A. K.; Lin, H.; Block, K. Differential Effects of Cholesterol and Lanosterol on Artificial Membranes. *Proc. Natl. Acad. Sci. U.S.A.* **1977**, *74*, 4924−4926.
(10) Dawson, J. H.; Sono, M. Cytochrome P-450 and Chloroperoxidase: Thiolate-Ligated Heme Enzymes. Spectroscopic Determination of Their Active Site Structures and Mechanistic Implications of Thiolate Ligation. *Chem. Rev.* **1987**, *87*, 1255−1276.
(11) Ruckpaul, K.; Janig, G. R.; Pfeil, D.; Honeck, H.; Blanck, J.; Smettan, G.; Rein, H.; Ristau, O.; Jung, C. Cytochrome P-450-Structure and Function. *Pharmazie* **1978**, *33*, 307−331.
(12) Poulos, T. L.; Finzel, B. C.; Hovvard, A. J. High-Resolution Crystal Structure of Cytochrome P450cam. *J. Mol. Biol.* **1987**, *195*, 687−700.
(13) Cupp-Vickery, J. R.; Poulos, T. L. Structure of Cytochrome P450eryF Involved in Erythromycin Biosynthesis. *Nat. Struct. Biol.* **1995**, *2*, 144−153.

(14) Hasemann, C. A.; Ravichandran, K. G.; Peterson, J. A.; Deisenhofer, J. Crystal Structure and Refinement of Cytochrome P450terp at 2.3 Å Resolution. *J. Mol. Biol.* **1994**, *236*, 1169−1185.
(15) Podust, L. M.; Poulos, T. L.; Waterman, M. R. Crystal Structure of Cytochrome P450 14α-sterol Demethylase (CYP51) from *Mycobacterium tuberculosis* in Complex with Azole Inhibitors. *Proc. Natl. Acad. Sci. U.S.A.* **2001**, *98* (6), 3068−3073.
(16) Ji, H.; Zhang, W.; Zhou, Y.; Zhang, M.; Zhu, J.; Song, Y.; Lu, J.; Zhu, J. A Three-Dimensional Model of Lanosterol 14α-Demethylase of *Candida albicans* and Its Interaction with Azole Antifungals. *J. Med. Chem.* **2000**, *43*, 2493−2505 and references therein.
(17) Lewis, D. F. V.; Wiesman, A.; Tarbit, M. H. Molecular Modelling of Lanosterol 14α-demethylase (CYP51) from *Saccharomices cerevisiae* via Homology with CYP102, a Unique Bacterial Cytochrome P450 Isoform: Quantitative Structure−Activity Relationships (QSARs) within Two Related Series of Antifungal Azole Derivatives. *J. Enzyme Inhib.* **1999**, *14*, 175−192.
(18) Tsukuda, T.; Shiratori, Y.; Watanabe, M.; Ontsuka, H.; Hattori, K.; Shirai, M.; Shimma, N. Modeling, Synthesis and Biological Activity of Novel Antifungal Agents (1). *Bioorg. Med. Chem. Lett.* **1998**, *8*, 1819−1824.
(19) Tafi, A.; Anastassopoulou, J.; Theophanides, T.; Botta, M.; Corelli, F.; Massa, S.; Artico, M.; Costi, R.; Di Santo, R.; Ragno, R. Molecular Modeling of Azole Antifungal Agents Active Against *Candida albicans*. 1. A Comparative Molecular Field Analysis Study. *J. Med. Chem.* **1996**, *39*, 1227−1235.
(20) Talele, T. T.; Kulkarni, V. M. Three-dimensional Quantitative Structure−Activity Relationships (QSAR) and Receptor Mapping of Cytochrome P-450$_{14\alpha DM}$ Inhibiting Azole Antifungal Agents. *J. Chem. Inf. Comput. Sci.* **1999**, *39* (2), 204−210.
(21) Buchel, K. H.; Draber, W.; Regel, E.; Plempel, M. Synthesen und Eigenschften von Clotrimazol und Weiteren Antimykotischen 1-Triphenylmethylimidazolen (Syntheses and Properties of Clotrimazole and Further Antimycotic 1-(Triphenylmethyl)imidazoles). *Arzneim.-Forsch.* **1972**, *22*, 1260−1272.
(22) Heeres, J.; Backx, L. J. J.; Mostmans, J. H.; Van Cutsem, J. Antimycotic Imidazoles. 4. Synthesis and Antifungal Activity of Ketoconazole, a New Potent Orally Active Broad Spectrum Antifungal Agent. *J. Med. Chem.* **1979**, *22*, 1003−1005.
(23) Heel, R. C.; Brodgen, R. N.; Carmine, A.; Morley, P. A.; Speight, T. M.; Avery, G. S. Ketoconazole: A Review of Its Therapeutic Efficacy in Superficial and Systemic Fungal Infections. *Drugs* **1982**, *23*, 1−36.
(24) Plempel, M.; Regel, E.; Buchel, K. H. Antimycotic Efficacy of Bifonazole in Vitro and in Vivo. *Arzneim.-Forsch.* **1983**, *33*, 517−524.
(25) Massa, S.; Di Santo, R.; Mai, A.; Botta, M.; Artico, M.; Panico, S.; Simonetti, G. Research on Antibacterial and Antifungal Agents. XIII. Synthesis and Antimicrobial Activity of 1-Arylmethyl-4-aryl-1H-pyrrole-3-carboxylic acids. *Farmaco* **1990**, *45*, 833−846.
(26) Massa, S.; Di Santo, R.; Retico, A.; Artico, M.; Simonetti, N.; Panico, S.; Fabrizi, G.; Lamba, D. Antifungal Agents. 1. Synthesis and Antifungal Activities of Estrogen-Like Imidazole and Triazole Derivatives. *Eur. J. Med. Chem.* **1992**, *27*, 495−502.
(27) Massa, S.; Di Santo, R.; Artico, M.; Costi, R.; Di Filippo, C.; Simonetti, G.; Retico, A.; Artico, M. Researches on Antibacterial and Antifungal Agents. XV. 3-Aryl-4-[α-(1H-imidazol-1-yl)benzyl]pyrroles with Potent Antifungal Activity. *Eur. Bull. Drug Res.* **1992**, *1*, 12−17.
(28) Massa, S.; Di Santo, R.; Artico, M.; Costi, R.; Apuzzo, G.; Simonetti, G.; Artico, M. Novel *In Vitro* Highly Active Antifungal Agents with Pyrrole and Imidazole Moieties. *Med. Chem. Res.* **1992**, *2*, 148−153.
(29) Di Santo, R.; Massa, S.; Artico, M. Synthesis of Biologically Active Azoles *via* TosMIC. *Farmaco* **1993**, *48*, 209−229.
(30) Massa, S.; Di Santo, R.; Costi, R.; Simonetti, G.; Retico, A.; Apuzzo, G.; Artico, M. Antifungal Agents. III. Naphthyl and Thienyl Derivatives of 1H-Imidazol-1-yl-4-phenyl-1H-pyrrol-3-ylmethane. *Farmaco* **1993**, *48*, 725−736.
(31) Massa, S.; Di Santo, R.; Costi, R.; Mai, A.; Artico, M.; Retico, A.; Apuzzo, G.; Artico, M.; Simonetti, G. Antifungal Agents. 4. Synthesis of *neo*-Isopyrrolnitrin and other 3-Aryl-4-nitro-1H-pyrroles *via* TosMIC. *Med. Chem. Res.* **1993**, *3*, 192−199.
(32) Artico, M.; Massa, S.; Di Santo, R.; Costi, R.; Retico, A.; Apuzzo, G.; Simonetti, N. Antifungal Agents. 5. Chloro and Amino Derivatives of 1,2-Diaryl-1-(1H-imidazol-1-yl)ethane with Potent Antifungal Activities. *Eur. J. Med. Chem.* **1993**, *28*, 715−720.
(33) Di Santo, R.; Massa, S.; Costi, R.; Simonetti, G.; Retico, A.; Apuzzo, G.; Troccoli, F. Antifungal Agents. VIII. Synthesis and Antifungal Activities of Bipyrryl Analogues of Bifonazole. *Farmaco* **1994**, *49*, 229−236.
(34) Artico, M.; Di Santo, R.; Costi, R.; Massa, S.; Retico, A.; Artico, M.; Apuzzo, G.; Simonetti, G.; Strippoli, V. Antifungal Agents. 9. 3-Aryl-4-[α-(1H-imidazol-1-yl)arylmethyl]pyrroles: A New Class of Potent Anti-*Candida* Agents. *J. Med. Chem.* **1995**, *38*, 4223−4233.
(35) Di Santo, R.; Costi, R.; Artico, M.; Massa, S.; Musiu, C.; Scintu, F.; Putzolu, M.; La Colla, P. Antifungal estrogen-like imidazoles. Synthesis and antifungal activities of thienyl and 1H-pyrrolyl derivatives of 1-aryl-2-(1H-imidazol-1-yl)ethane. *Eur. J. Med. Chem.* **1997**, *32*, 143−149.
(36) Di Santo, R.; Costi, R.; Artico, M.; Massa, S.; Musiu, C.; Milia, C.; Putzolu, M.; La Colla, P. N-(1-Naphthylmethyl)-N-(1-alkyl-4-aryl-1H-pyrrol-3-ylmethyl)methylamines Related to Naftifine. Synthesis and Antifungal Activity. *Med. Chem. Res.* **1997**, *7*, 98−108.
(37) *Catalyst*, version 4.6; Molecular Simulation Inc., 9685 Scranton Road, San Diego, CA 92121-3752.
(38) Kaminski, J. J.; Rane, D. F.; Snow, M. E.; Weber, L.; Rothofsky, M. L.; Anderson, S. D.; Lin, S. L. Identification of novel farnesyl protein transferase inhibitors using three-dimensional database searching methods. *J. Med. Chem.* **1997**, *40*, 4103−4112.
(39) Barnum, D.; Greene, J.; Smellie, A.; Sprague, P. Identification of common functional configurations among molecules. *J. Chem. Inf. Comput. Sci.* **1996**, *36*, 563−571.
(40) Botta, M.; Corelli, F.; Gasparrini, F.; Messina, F.; Mugnaini, C. Chiral azole derivatives. 4.1. Enantiomers of bifonazole and related antifungal agents: synthesis, configuration assignment, and biological evaluation. *J. Org. Chem.* **2000**, *65* (15), 4736−4739.
(41) Catalyst guidelines, http://www.msi.com/support/catalyst/hypogen.html.
(42) Smellie, A.; Teig, S.; Towbin, P. Poling: promoting conformational variation. *J. Comput. Chem.* **1995**, *16*, 171−187.
(43) Davey, W.; Gwilt, J. R. Chalcones and Related Compounds. Part I. Preparation of Nitro-, Amino-, and Halogeno-chalcones. *J. Chem. Soc.* **1957**, 1008−1014.
(44) Rekhter, M. A.; Grushetskaya, G. N.; Panasenko, A. A.; Krimer, M. Z. New Derivatives of N-Vinyltriazoles-1,3-diaryl-3(1H-1,2,4-triazol-1yl)-2-propen-1-ones. *Khim. Geterotsikl. Soedin.* **1995**, *7*, 910−914; *Chem. Abstr.* **1996**, *124*, 202126k.
(45) Severi, F.; Costantino, L.; Benvenuti, S.; Vampa, G.; Mucci, A. Synthesis and Description of Chalcone-like Compounds, Inhibition of Aldose Reductase. *Med. Chem. Res.* **1996**, *6*, 128−136.
(46) Hahn, M. Three-dimensional shape-based searching of conformationally flexible compounds. *J. Chem. Inf. Comput. Sci.* **1997**, *37*, 80−86.
(47) Fischer, R. In *The design of experiments*; Hafner: New York, 1996.

JM011087H